Integrated Quantum Photonics

Alberto Politi, Jonathan C. F. Matthews, Mark G. Thompson, and Jeremy L. O'Brien

(Invited Paper)

***Abstract*—This paper reviews recent advances in integrated waveguide circuits, lithographically fabricated for quantum optics. With the increase in complexity of realizable quantum architectures, the need for stability and high quality nonclassical interference within large optical circuits has become a matter of concern in modern quantum optics. Using integrated waveguide structures, we demonstrate a high performance platform from which to further develop quantum technologies and experimental quantum physics using single photons. We review the performance of directional couplers in Hong–Ou–Mandel experiments, together with inherently stable interferometers with controlled phase shifts for quantum state preparation, manipulation, and measurement as well as demonstrating the first on-chip quantum metrology experiments. These fundamental components of optical quantum circuits are used together to construct integrated linear optical realizations of two-photon quantum controlled logic gates. The high quality quantum mechanical performance observed at the single photon level signifies their central role in future optical quantum technologies.**

***Index Terms*—Photonics, quantum optics, waveguides.**

I. Introduction

QUANTUM technologies offer significant opportunities for information and communication technologies, as well as profound insight into the fundamental workings of nature. This pioneering field of research is at the interface of physical and information science and promises to revolutionize information technology based on harnessing the unique properties of quantum mechanics to encode, transmit, and process information.

Quantum photonics is recognized as fundamental to explore quantum science and is expected to play a central role in advancing future technologies. Single photons are repeatedly used for breakthrough experiments verifying uniquely quantum mechanical phenomena together with many highly successful proof-of principle demonstrations of emerging quantum technologies, each offering profound improvement over their classical counterpart. To date, quantum photonic demonstrations have been realized using large-scale (bulk) optical elements, bolted onto sizeable optical benches in the laboratory. Due to the physical size and the inherent instability of these individual components, this approach now hinders the development of more complex quantum optical schemes, and currently prevents the realization of fully scalable quantum optic devices.

We review in this manuscript a novel approach for alleviating the issues of stability and allowing accurate control of the path length through the implementation of quantum optic circuits using photonics integrated waveguides. Our demonstrations of reliable and repeatable, high performance on a nonclassical single photon level within silica-on-silicon waveguide circuits begin a new line of research in quantum optics. The underlying components for quantum technologies based on linear optics (directional couplers (DCs) and Mach–Zehnder interferometers) are fabricated and verified to yield high-visibility nonclassical and classical interference, respectively. In turn, these components are used together to form multiphoton entangling gates [1] as well as the core components used for fully reconfigurable quantum circuits. The reconfigurable aspect of our devices allow us to perform integrated quantum metrology experiments to a high degree, by directly manipulating entangled states generated directly on-chip [2].

This review begins with an introductory background in quantum information science based on single photons. Section III describes the fabrication process and materials used to realize the single photon waveguide circuits, while the core integrated linear optical components are described in Section IV—describing the use of DCs to provide nonclassical interference—and in Section V—detailing the use of integrated Mach–Zehnder interferometers manipulating quantum states. Section VI brings together the constituent quantum waveguide components in the construction of two-photon quantum logic gates with the focus on an integrated realization of an optical quantum controlled-NOT gate. Section VII describes the future directions for integrated quantum optical devices. Section VIII summarizes and concludes the paper.

II. Photonic Quantum Information Science

To date, the principles of quantum mechanics provide deep physical understanding into the nature of matter and light on the atomic and subatomic scale, yielding prediction and subsequent observation of wave-particle duality in systems, and phenomena such as a single entity existing in superposition of multiple distinct states and nonlocal, instantaneous interaction between many entangled systems, referred famously by

Manuscript received February 20, 2009; revised April 12, 2009. This work was supported by the Intelligence Advanced Research Projects Activity, the Engineering and Physical Sciences Research Council, the Quantum Information Processing Interdisciplinary Research Collaboration, and by the Leverhulme Trust.

A. Politi, J. C. F. Matthews, and J. L. O'Brien are with the Centre for Quantum Photonics, H. H. Wills Physics Laboratory and Department of Electrical and Electronic Engineering, University of Bristol, Bristol, BS8 1UB, U.K. (e-mail: alberto.politi@bristol.ac.uk; jonathan.matthews@bristol.ac.uk; jeremy.obrien@bristol.ac.uk).

M. G. Thompson is with the Centre for Quantum Photonics, H. H. Wills Physics Laboratory and Department of Electrical and Electronic Engineering, University of Bristol, Bristol, BS8 1UB, U.K., and also with the Toshiba Research and Development Centre, Kawasaki 212-8582, Japan (e-mail: Mark.Thompson@Bristol.ac.uk).

Color versions of one or more of the figures in this paper are available online at http://ieeexplore.ieee.org.

Digital Object Identifier 10.1109/JSTQE.2009.2026060

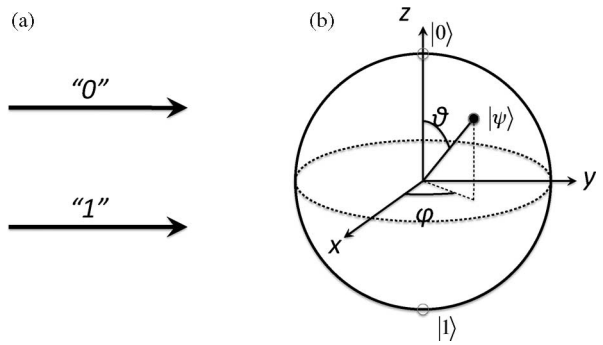

Fig. 1. (a) Logical states of a classical bit. (b) Arbitrary state of a quantum qubit may be represented as any position on the surface (in the case of pure states) or within (for mixed states) the Bloch sphere.

Einstein as "spooky action at a distance" [3]. Through exploring fundamental quantum physics and employing uniquely quantum mechanical properties, quantum information science (QIS) aims to develop areas of technology far beyond capabilities based on classical physics alone.

The profound improvements dealt by quantum mechanics over classical physics have lead to new areas of computer science and mathematical physics and to develop the theory of perhaps one of the most enthralling applications of quantum physics: the construction of a quantum computer [4]. Among the already vast field of quantum computation and information, theoretical work predicts a quantum computer will change complexity classes of certain problems, for example Shor's algorithm for factorizing the product of two prime numbers exponentially faster than a classical computer [5]—a task previously thought to take an exponential number of resources for solution, and hence, the basis for current classical cryptography protocols.

The underlying element on which QIS is based is the qubit: the basic measure of quantum information represented by any two level quantum system. Consider for example, two energy levels of an atomic system labeled by either "0" or "1". Classical information theory considers levels equivalent to classical "bits" whose logical state are either 0 or 1 [as shown in Fig. 1(a)]. If, however, we encode a qubit onto this system by using the atomic system, then the state of the qubit could exist in either of the quantum states $|0\rangle$ or $|1\rangle$, as with the classical model; more generally quantum mechanics allows the qubit's pure state to be in some complex linear combination of both channels given by

$$|\psi\rangle = \cos\theta\,|0\rangle + e^{i\phi}\sin\theta\,|1\rangle\,. \tag{1}$$

A geometrical representation for qubit states is represented by a Euclidean 3-D sphere known as the Bloch sphere, as shown in Fig. 1(b).

Several staggering challenges exist on the road to developing a fully functional and practical quantum computer. Physically realizable and scalable qubits must be developed that can be accurately controlled, measured and prepared to interact in two-qubit entangling gates in order to complete a universal set of quantum logic gates. At the same time, the quantum state of qubits must be separated from the environment to such a degree to avoid decoherence or collapse of each qubits state into classical information [6]. Many physical implementations are under development to fulfill these criteria for a viable qubit, including nuclear magnetic resonance, trapped ions, neutral atom approaches, cavity quantum electrodynamics, solid state, and semiconductors [7].

One of the leading approaches for implementing quantum information science is quantum photonics—the science of single photons. The accurate control of photonic quantum states, for example, polarization control using commercially available waveplates, yields the relative simplicity with which to construct any single qubit logic gate [8]. Furthermore, photons lack the problematic interaction between qubit and environment, which hinders other implementations and strengthens the photon's promise as a "flying" communication qubit. In 2001, it was proven by Knill, Laflame, and Milburn (KLM) that linear optical components, together with single photon detectors and single photon sources, are sufficient to build a fully scalable quantum computer [9], and hence, yielding the exciting prospect of all-optical quantum technologies. Since then, photonics has accelerated in presenting many successful demonstrations including improved information security given by quantum cryptography [10], [11]; beating the shot noise limit for increased measurement resolution in quantum metrology [12]–[16]; enhanced resolution beyond the diffraction limit in quantum lithography [17], [18] together with implementing key proof-of-principle demonstrations for the quantum computer including crucial quantum gates [19] and simple algorithms [8].

As well as developing quantum technologies, photonics has contributed significantly in experimentally verifying and understanding quantum mechanics. One of the fundamental phenomena forming a basis for quantum technologies is entanglement: the theory describing nonlocal behavior of correlated systems whose quantum state cannot be fully described individually. Entanglement provides an explanation for the famous Einstein–Podolsky–Rosen Gedanken experiment [20] via Bell inequality [21] violations, which were first experimentally demonstrated using photons [22]–[25]. These demonstrations crucially verify entanglement theory, vital for quantum protocols including quantum teleportation (central to the KLM scheme), which was first demonstrated in photonics [26], [27] along with superdense coding [28] and large entangled systems known as graph or cluster states [29], [30]—the latter forming so called "one-way" quantum computation.

These important implementations of experimental quantum information science have primarily consisted of large-scale (bulk) optical elements confined to optical laboratories, making such schemes physically unscalable, sensitive to stability and impractical for applications outside of the research laboratory. In addition, many have required the design of sophisticated interferometers to achieve the subwavelength stability required for reliable operation. Continuing mainstream activities are developing large scale quantum systems that are becoming too large and unstable to be realistically implemented under these experimental constraints. This paper reviews a novel solution to achieving compact, efficient and stable quantum optics experiments.

III. Silica on Silicon for Quantum Information

The silica material system is a natural choice for the development of quantum integrated photonic circuits since it exhibits low waveguide losses (<0.1 dB/cm), couples efficiently to single mode optical fiber and is transparent at wavelengths that match the current state-of-the-art in single photon generation and detection [31]. As in conventional (or classical) integrated optics devices, the light is guided in waveguide structures consisting of a "core" that is surrounded by a slightly lower refractive index "cladding" (analogous to an optical fiber). These waveguide can be designed to support only a single transverse mode for a given wavelength range, and also to match closely the mode profile of an optical fiber (allowing efficient coupling of photons to fiber-coupled single photon sources and detectors).

The silica waveguide technology, or planar lightwave circuit (PLC) technology, offers the possibility of integrating a number of passive functions on a single silicon chip [32]. An important example of such functions is optical modulation using the thermooptic effect. Being able to control optical phases on a chip is crucial for a number of classical and quantum applications. The stability with which the thermo-optic effect allows control of optical phase, in combination with polarization-insensitive operation, is the reason why the PLC technology is already been used for quantum communication experiments [33], [34]. In these experiments, unbalanced integrated Mach–Zehnder interferometers were used to analyze time-bin encoded photons to implement quantum key distribution protocols. While these beautiful demonstrations are fundamental for quantum communication operations, they do not prove the capability of PLC in other quantum optics applications, where multiphoton nonclassical interference is required. In the remainder of this paper, we will focus on the demonstration of nonclassical interference in integrated silica devices and their application to quantum optics experiments.

The operating wavelength of choice is $\lambda \sim 800$ nm, where commercial silicon avalanche photodiode single photon counting modules (SPCMs) are near their peak efficiency of $\sim$70%. Low waveguide loss and single mode operation for waveguide dimensions comparable to the core size of conventional single mode optical fibers at $\sim$800 nm (4–5 μm) are achieved using standard photo lithography fabrication techniques and low level doping to control the refractive index of silica.

The waveguide structure used is illustrated in cross section shown in Fig. 2. A refractive index contrast of $\Delta = 0.5\%$ was chosen to give single mode operation at 804 nm for $3.5 \times 3.5\ \mu$m waveguides.[1] This value of Δ provides moderate mode confinement [the transverse intensity profile is shown in Fig. 2(a)] thereby minimizing the effects of fabrication or modeling imperfections. The devices were fabricated on a 4 in silicon wafer (material *I*), onto which a 16 μm layer of thermally grown undoped silica was deposited as a buffer (II) to form the lower cladding of the waveguides. The core was formed from 3.5 μm layer of silica doped with germanium and boron oxides which

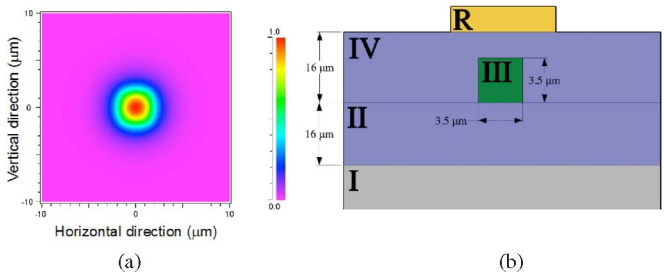

Fig. 2. Silica on silicon waveguide for quantum photonic circuits. (a) Simulation of the transverse profile of the guided mode in the waveguide. (b) Schematic of the structure of the chip.

was deposited by flame hydrolysis. The 3.5 μm wide waveguides structures were patterned into this core layer via standard optical lithographic techniques (III). An upper cladding (IV) of 16 μm was overgrown in phosphorus and boron-doped silica. This layer had a refractive index matched to the lower cladding layer. Metal patterned on the top of the devices provided resistive heaters, metal connections and contact pads that can be used to control locally the temperature of part of the chip. The wafer was diced into individual chips, each containing typically several devices. The facets of some chips were polished to enhance coupling of photons from fibers to the input and output waveguides.[2]

A number of devices were designed and fabricated, including DCs with various coupling ratio, Mach–Zehnder interferometers (consisting of two DCs), and more sophisticated devices built up from several DCs with different reflectivities.[3]

The experiments we review were conducted using degenerate single photon pairs at a wavelength of 780 or 804 nm produced via spontaneous parametric down conversion (SPDC) from a type I phase matched bismuth borate (BiB_3O_6) (BiBO) nonlinear crystal. The crystal was pumped using a 402 nm continuous wave (CW) laser for two-photon experiments, or by a 390 nm, 150 fs pulsed laser beam for multiphoton experiments. The 390 nm pump was prepared using a further BiBO crystal, phase matched for second harmonic generation (SHG) to double the frequency of a 780 nm mode-locked Ti:Sapphire laser. Degenerate photon pairs created by the SPDC crystal pass through 3 nm interference filters and are collected into single mode polarization maintaining fibers (PMFs). The photons coupled in the PMFs were launched into the chip and then collected at the outputs using two arrays of eight PMFs, with 250 μm spacing, to match that of the waveguides, and detected with fiber-coupled SPCMs. The PMF arrays and chip were directly buttcoupled, with index matching fluid, to obtain an overall coupling efficiencies of $\sim$70% through the device (input+output insertion losses = 30%, propagation losses are negligible). Fig. 3 shows a schematic picture of the source and the fiber array used to couple the photons into and out the desired chip.

[1] As determined by modeling with the vectorial mode solving package Fimmwave.

[2] All devices were fabricated at the Centre for Integrated Photonics.

[3] We used Rsoft's beam propagation method (BPM) package.

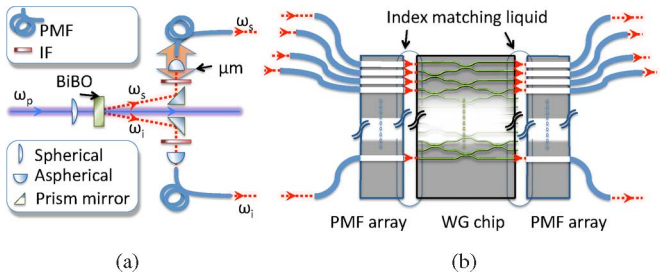

Fig. 3. Schematic representation of (a) single photon source and (b) experimental setup used to couple the photons into the integrated circuit.

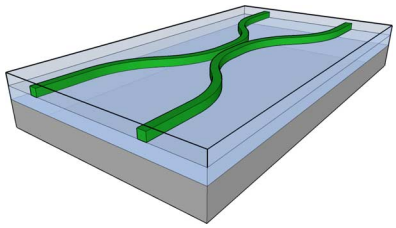

Fig. 4. Schematic of an integrated DC.

IV. Directional Couplers

In quantum optical architectures, information is encoded onto single photons propagating in superposition along multiple optical paths or "modes." The heart of quantum processing is, therefore, a linear optical network based on classical and (quantum) nonclassical interference [35] between photons to split and combine optical modes. In conventional large-scale (bulk) optical implementation of linear networks, photons propagate in free space and optical circuits are constructed using standard mirrors and "partially reflective mirrors" or beam splitters (BS). Such devices act on individual photons so that their state evolves into superposition of many paths, and nonclassical interference between two or more photons can be achieved. High contrast classical interference requires stability of optical path length on a subwavelength scale, demanding the realization of stable interferometers; high quality quantum interference, signified by the visibility between quantum and classical statistics, demands high indistinguishability of the incident photons, including the exact overlap of optical modes. The quality of classical and nonclassical interference, together with the photonic loss through a linear optical circuit, determines the performance of a given quantum optical circuit.

To realize operations between optical modes, as in free space beam splitters (BS), it is possible to fabricate DC: when two waveguides approach each other the evanescent fields of the two structures overlap and coupling between waveguide is achieved (see Fig. 4). The coupling ratio of the DC ($1-\eta$, where η is equivalent to BS reflectivity) can be lithographically tuned by varying the separation between the waveguides and the length of the coupler region. From the quantum information perspective, DCs can be described by an unitary operation acting on the input/output modes, as

$$U_{\mathrm{DC}} \doteq \begin{pmatrix} \sqrt{\eta} & i\sqrt{1-\eta} \\ i\sqrt{1-\eta} & \sqrt{\eta} \end{pmatrix}. \tag{2}$$

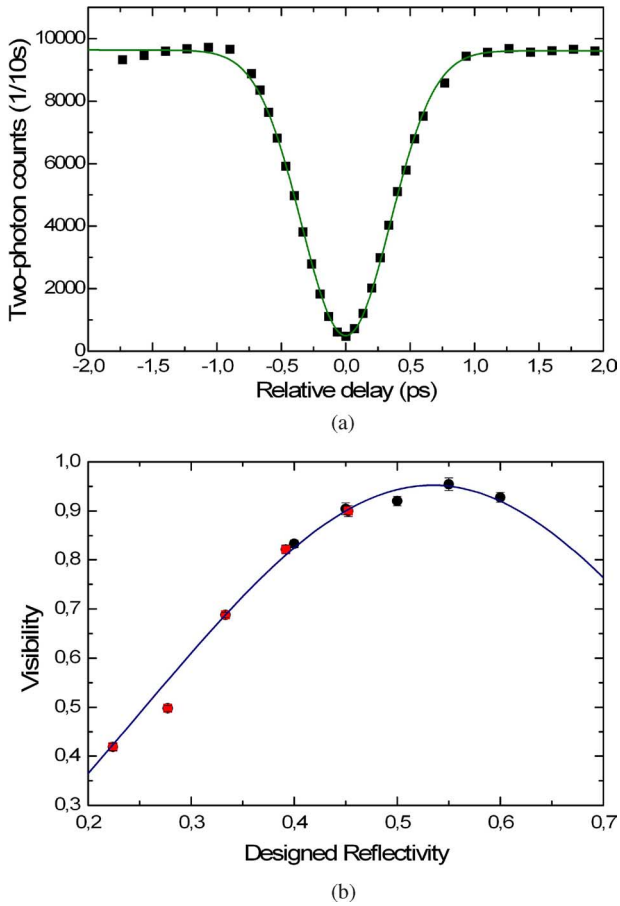

Fig. 5. Two-photon quantum interference in integrated DCs. Part (a) Shows the variation of coincidental two-photon detections as function of the relative delay of the two photons launched in the coupler. (b) Quantum interference visibility as a function of the designed reflectivity of the coupler. Black points refer to $1/2$ couplers and red dots to $1/3$ coupler, as explained in the text. For both the plots error bars are smaller then data points.

Note that for $\eta = 1/2$, the DC is equivalent to a Hadamard gate H

$$H \doteq \frac{1}{\sqrt{2}} \begin{pmatrix} 1 & 1 \\ 1 & -1 \end{pmatrix} \tag{3}$$

up to local σ_z rotations.

To demonstrate that silica on silicon technology is an excellent candidate to implement quantum circuits, it is necessary to show that it is possible to achieve quantum interference between single photons. Fig. 5(a) shows the rate of coincidental detection of two photons at the output waveguides of a DC as arrival time delay between the photons is changed. The expected dip near zero delay in relative photon arrival time [35] indicates the quantum behavior of the system. The depth of such a dip indicates the degree of quantum interference, which can be quantified by the visibility $V = (N_{\max} - N_{\min})/N_{\max}$. Ideally, the visibility is a function of the reflectivity η

$$V_{\mathrm{id}} = \frac{2\eta(1-\eta)}{1-2\eta+2\eta^2} \tag{4}$$

and in experiments it can be reduced by any process that limits the indistinguishability of the single photons. The measured

visibility $V = 94.8 \pm 0.5\%$ quantifies the quality of the interference and demonstrates very good quantum behavior of photons in an integrated optics architecture.

Fig. 5(b) shows the measured visibility for the quantum interference for ten couplers on a single chip with a range of design ηs from 0.22 to 0.6. A best fit was performed on the experimental data points to produce the curve in the figure. The theoretical model has two fitting parameters: one to take into account mode mismatch, that provides deviation from the ideal relation of (4); the other includes the difference between the designed and real reflectivity of the coupler. The latter parameter, found to be $\delta\eta = 3.4 \pm 0.7\%$, does not introduce any limitation of the quantum interference, but give a small translation of the curve to the right. The mode mismatch parameter is used to include the nonperfect visibility of the quantum interference. The best fit, however, does not give any information about the reason for the mode mismatch, since a mode mismatch in any degree of freedom is completely equivalent to mode mismatch in any other degree of freedom [36]. Some of the possible phenomena that can contribute to the reduced visibility are: polarization mismatch given by misalignment of PMF fibers in the array (specified to be $< 3^\circ$); spatial mode mismatch given by weakly guided higher order modes propagating across the relatively short devices; frequency mismatch given by a nonperfect filtering of the photons at the source. The average relative visibility $V_{\rm av} = 1/N \sum_i^N V/V_{\rm id}$, a measure of the global performance of the couplers, was found to be $V_{\rm av} = 95.0 \pm 0.8$. These results demonstrate the high yield and excellent reproducibility of the devices for quantum optic applications.

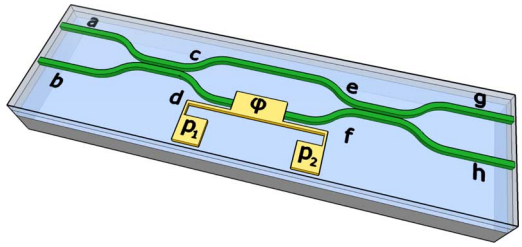

Fig. 6. Schematic of an integrated Mach–Zehnder interferometer with a variable phase shifter realized using a resistive heater.

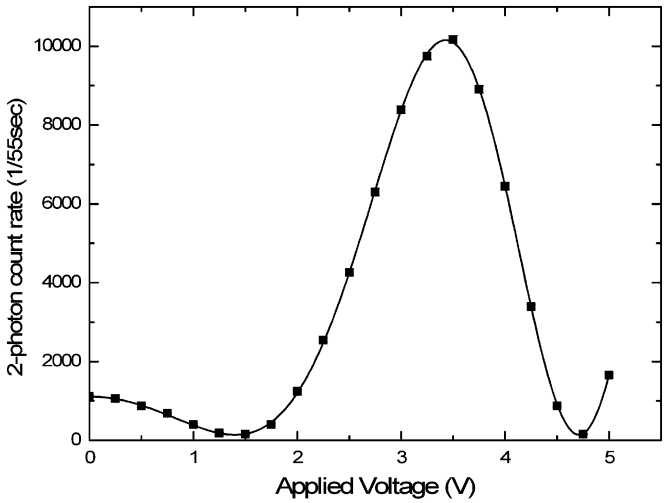

Fig. 7. Calibration of the Mach–Zehnder interferometer: rate of two-photon coincidental detection varying the voltage applied to the resistive heater.

V. Mach–Zehnder Interferometers

Integrated arbitrary qubit preparation is a key capability for both the development and characterization of integrated photonic quantum devices. Mathematically, it is possible to map arbitrarily from the logical qubit $|0\rangle$ to the general state $\cos\phi/2\,|0\rangle + e^{-i\theta}\sin\phi/2\,|1\rangle$ by applying the operation $U_{\rm prep} = e^{i\theta\sigma_Z/2} H e^{i\phi\sigma_Z/2} H$ and controlling the two real free parameters $\theta \in [0, 2\pi)$ and $\phi \in [0, \pi)$, where H is the Hadamard operation and σ_Z is the third Pauli operator. The unitary nature of quantum mechanics therefore allows $U_{\rm prep}$ to map from the computational basis $\{|0\rangle, |1\rangle\}$ to any other given basis, while the inverse operation $U_{\rm prep}^\dagger$ provides the reverse mechanism allowing the projective measurement of single qubit states in arbitrary bases, and hence, full process tomography of quantum circuits [37].

For polarization-encoded photons, the operation $U_{\rm prep}$ is realized in bulk optics by using, for example, combinations of commercially available quarter- and half-waveplates. For dual rail-encoding, the equivalent implementation requires one 50% reflective nonpolarizing beam splitter for each Hadamard operation H and accurate control over the relative optical phase between the two optical paths to realize each phase gate $e^{i\phi\sigma_z}$. The accurate realization of the $He^{i\phi\sigma_Z/2}H$ term is, therefore, locally equivalent to a Mach–Zehnder interferometer, where each optical mode of the input entering the first DC is transformed into a superposition across modes c and d: *eg* $|1\rangle_a|0\rangle_b \rightarrow |1\rangle_c|0\rangle_d + i|0\rangle_c|1\rangle_d$. The relative optical phase is controlled by the parameter ϕ—i.e., $|1\rangle_c|0\rangle_d + i|0\rangle_c|1\rangle_d \rightarrow |1\rangle_c|0\rangle_d + e^{i\phi}i|0\rangle_c|1\rangle_d$—before the two modes are recombined at the second coupler. Any small variation in the relative optical path of the interferometer hinders the accurate control of the phase ϕ, and hence, renders such a scheme realized using individual bulk optical components inherently unstable such that it will not scale favorably for incorporation into larger and more complicated experiments and devices. The monolithic nature of integrated waveguide optics using 50% splitting ratio DCs solves the problem of constructing completely stable Mach–Zehnder interferometers (see Fig. 6), and local control of the phase between the waveguides inside the interferometer enable accurate control over the output state. It is interesting to note that the mathematical description of quibit rotations can be generalized to states that live in bigger Hilbert spaces. If we use the path encoding to describe an N-dimensional state over N waveguides, it is possible to use several Mach–Zehnder interferometers and additional phase shifters to realize any arbitrary N-mode unitary operator [38].

The metallic layer deposited on the top of the silica chip is used to provide resistive heaters, metallic connections and contacts to physically control the phase inside the interferometer. When a voltage is applied across the contact pads p_1 and p_2,

current flows through R and generates heat which dissipates into the device and locally raises the temperature T of the waveguide structure directly beneath R. A change in the temperature of the waveguide provides a temperature change in its core and cladding. To first approximation, the change in refractive index n of silica is given by $dn/dT = 10^{-5}/\mathrm{K}$, independently of the compositional variation of core and cladding [39]. This induces a change in the mode group index of the light, and therefore, a phase difference ϕ with respect to the unperturbed waveguide. The devices were designed to enable a continuously variable phase shift and, thanks to the monolithic nature of the device, no strict global temperature control of the chip is required.

The voltage-controlled phase inside the interferometer circuit is defined by a nonlinear relation $\phi(V)$ that depends on the characteristics of each chips. For this reason, each device had to be calibrated to relate the applied voltage to the phase difference introduced in the interferometer. We used a two photon experiment to find the $\phi(V)$ relation. One photon was launched into each of the ports a and b of the device so that the maximally entangled two photon Fock state $|2\rangle_c |0\rangle_d + |0\rangle_c |2\rangle_d$ is generated inside the chip. Controlling the phase ϕ in the device, the phase of the entangled state is altered according to $|2\rangle_e |0\rangle_f + e^{2i\phi} |0\rangle_e |2\rangle_f$. In comparison to one-photon interference, this "quantum calibration" experiment utilizes the reduced de Broglie wavelength [13]–[15] to reduce the error of the $\phi(V)$ relation. This is because it is possible to test a wider sample of the interference fringe, since the set of the value of the phase ϕ can assume is limited by the maximal voltage (current) that it is possible to apply to the resistive heater. In first approximation, the applied phase ϕ is proportional to the power dissipated by the resistor. This translates into a quadratic relation between the applied voltage and the phase. To take into account deviations from the ideal case, mainly given by nonohmic behavior, we fixed the form of the $\phi(V)$ relation as

$$\phi(V) = \alpha + \beta V^2 + \gamma V^3 + \delta V^4. \tag{5}$$

A best fit analysis on the two-photon interference data was performed to calculate the parameters in the $\phi(V)$ relation.

After the calibration process, it was possible to measure the interference pattern of single photon detections at the two outputs of the circuit when launching single photons into one input of the integrated device and varying the phase ϕ. As the phase of one waveguide is changed by applying a voltage across the resistive heater, the probability of detecting photons at the outputs g and h varies according to $P_g = 1/2\,[1 - \cos(\phi)]$ and $P_h = 1/2\,[1 + \cos(\phi)]$. The observed fringes, shown in Fig. 8(a), show a high contrast $C = (\max - \min)/(\max + \min)$ of $C = 98.2 \pm 0.3\%$. From the contrast value, it is possible to calculate how well this device would perform if used to prepare path-encoded states. This is described by the average fidelity between the measured and ideal output state $U_{\mathrm{MZ}} |0\rangle = \cos(\phi/2) |0\rangle + \sin(\phi/2) |1\rangle$. Assuming no mixture or complex phase is introduced and averaging over the range $\phi \in [-\pi/2, \pi/2]$, we found the average fidelity to be $F = 99.984 \pm 0.004\%$.

Phase control capability is also important for the on-chip generation, manipulation, and analysis of entangled quantum states.

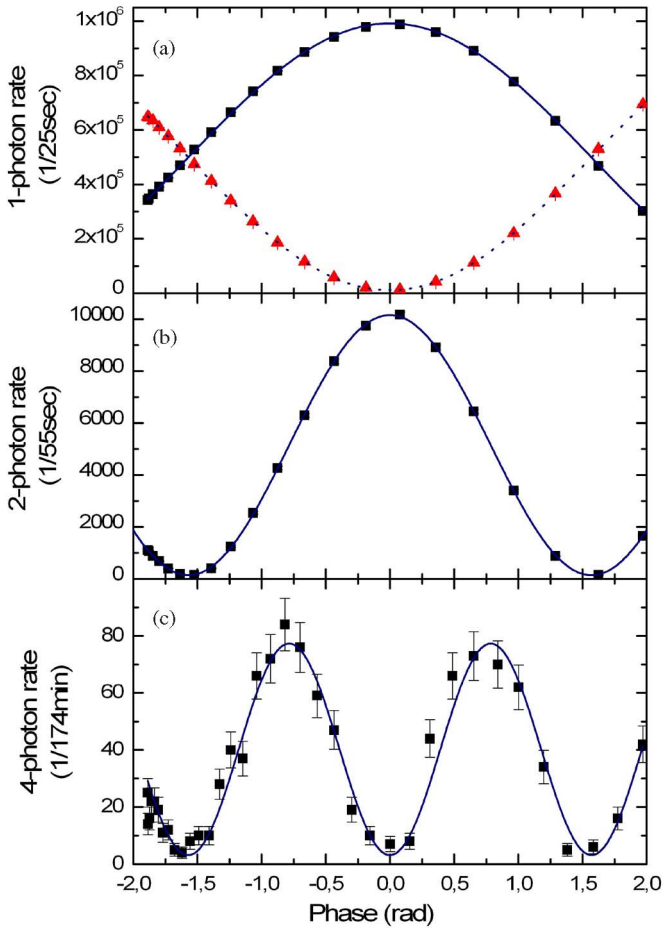

Fig. 8. Integrated quantum metrology. (a) Single photon count rates in the outputs g and h as the phase $\phi(V)$ is varied. (b) Two-photon coincidental count rate between the outputs g and h when the state $|1\rangle_a |1\rangle_b$ is launched in the interferometer and varying the phase $\phi(V)$. (c) Four-photon detection rate of the output state $|3\rangle_g |1\rangle_h$ when inputting the four-photon state $|2\rangle_a |2\rangle_b$.

By inputting the indistinguishable two-photon state $|1\rangle_a |1\rangle_b$ into the first DC of the Mach-Zehnder circuit, the two-photon maximally entangled state $|2\rangle_c |0\rangle_d + |0\rangle_c |2\rangle_d$ is generated inside the device. Through controlling the phase ϕ, the entangled state is altered according to $|2\rangle_e |0\rangle_f + e^{2i\phi} |0\rangle_e |2\rangle_f$. Simultaneous detection of a single photon at each output yields a two-photon interference fringe with twice the frequency of one-photon interference, according to $P_{g,h} = 1/2\,(1 + \cos 2\phi)$. We show such two-photon interference fringe in Fig 8(b), which plots the measured two-photon coincidence rate as a function of the phase ϕ. The curve shows a contrast of $C = 97.2 \pm 0.4\%$, greater than the threshold of $C_{\mathrm{th}} = 1/\sqrt{2}$ required to beat the shot noise limit for two-photons [13], [15], [40], [41].

The accuracy and stability with which the resistive heater controls the phase inside an integrated waveguide MZ interferometer, as shown by the one- and two-photon interference fringes, leads to applications in technologies such as quantum metrology. As a proof of principle, this requires demonstration using maximally entangle N 0 0 N states of the form $|N\,0\rangle + |0\,N\rangle$ (expressed as a photon number Fock state in two paths) [42]. Unfortunately, for N larger than 2, it is not currently simple

to directly generate such states using photons produced with SPDC and linear optical circuits in a deterministic manner [40]. It is, however, possible to solve this problem by post-selecting the presence of the maximally entangled 4-N00N state: by inputting the state $|2\rangle_a |2\rangle_b$ into the interferometer, nonclassical interference at the first DC produces the state

$$\sqrt{3/4}\left(|4\rangle_c |0\rangle_d + |0\rangle_c |4\rangle_d\right)/\sqrt{2} + 1/\sqrt{4}\,|2\rangle_c |2\rangle_d . \quad (6)$$

At the second DC, only the $|4\rangle_c |0\rangle_d + |0\rangle_c |4\rangle_d$ part of the state in (6) gives rise to either of the terms $|3\rangle_e |1\rangle_f$ or $|1\rangle_e |3\rangle_f$ in the output state of the interferometer. By detecting either of the states $|3\rangle_e |1\rangle_f$ or $|1\rangle_e |3\rangle_f$ (by cascading three detectors using 1×2 fiber-beam splitters on either outputs g or h of the device) a $\lambda/4$ interference fringe can be observed [15], [43]. By varying the phase of the interferometer by ϕ, the probability to detect the 3:1 pattern has a period of $\phi/2$. The measured interference pattern is shown in Fig. 8(c), which plots fourfold detections corresponding to the detection of the $|3\rangle_g |1\rangle_h$ against the phase ϕ of the device. The contrast of the fourfold interference fringe is $C = 92 \pm 4\%$. Despite the postselection scheme, this is still sufficient to beat the shot noise limit [41].

In addition to single photon interference in interferometers, nonclassical interference of two photons can be investigated in integrated devices in a similar manner, as described in the previous section. DCs offer high performance and stable results for quantum optics operations. In these devices, the reflectivity η is set in the fabrication process. However, more general photonic circuits, including adaptive schemes whose function depends on the input state, such as Fock state filters [44], [45], make use of devices equivalent to a single coupler with variable η. Reconfigurable photonic circuits, including routing of photons, can be realized by combining such variable η devices. By controlling the phase ϕ within our devices, we can specify the unitary operation

$$U_{\mathrm{MZ}} \doteq \begin{pmatrix} \sin(\phi/2) & \cos(\phi/2) \\ \cos(\phi/2) & -\sin(\phi/2) \end{pmatrix} \quad (7)$$

when acting on an arbitrary superposition of the two input paths. This operation is equivalent to a single coupler with variable reflectivity

$$\eta = \sin^2\left(\frac{\phi}{2}\right). \quad (8)$$

We performed multiple quantum interference experiments in which two photons were launched into inputs a and b of the device. While scanning through the relative arrival time with an off-chip optical delay, we measured the rate of simultaneous detection of a single photon at both outputs g and h. Each experiment resulted in a quantum interference "dip" in this rate of simultaneous photon detection. The main panel in Fig. 9 plots the quantum interference visibility observed for different values of ϕ and hence η. In Fig. 9, we also show two examples of the raw data used to generate this curve: Fig. 9(c) $\phi = -0.49 \pm 0.01$ rad, $V = 0.129 \pm 0.009$; Fig. 9(b) $\phi = -1.602 \pm 0.01$ rad, $V = 0.982 \pm 0.009$.

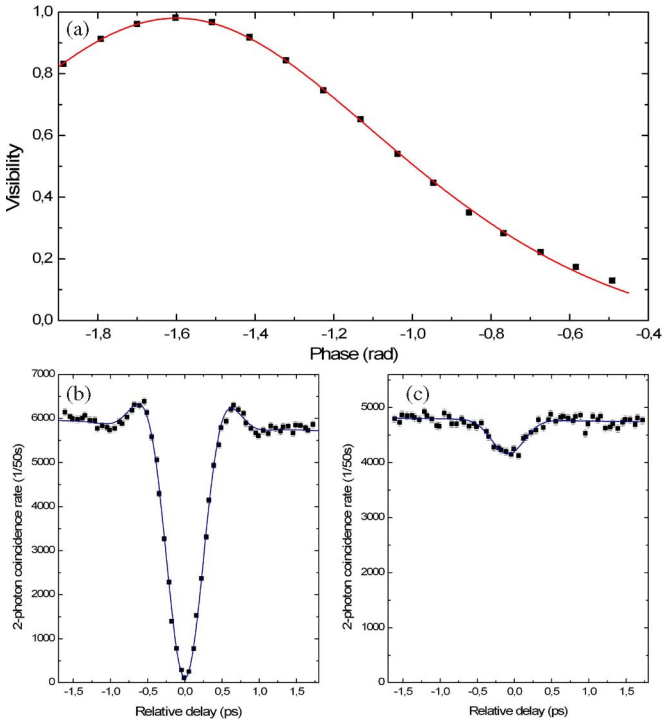

Fig. 9. Controlling the degree of quantum interference on a single chip. (a) Visibility of the quantum interference versus applied phase in the integrated Mach–Zehnder interferometer. The solid line is a theoretical fit with only a phase-offset and a single mode-mismatch as the free parameters. (b) High visibility two-photon interference for $\phi = -1.602 \pm 0.01$ rad. (c) Low visibility two-photon interference for $\phi = -0.49 \pm 0.01$ rad. The best fit function in both plots takes into account the non-Gaussian shape of the interference filter used in the experiment.

VI. Controlled-NOT (C-NOT) Gate

As explained in the introduction, entanglement is fundamental for quantum information processing as well as for quantum science in general. For this reason, any candidate technology for quantum applications needs to prove the ability of generating entangled states. An example of a quantum circuit capable of manipulating the state of two qubit in such a way that the final output can be entangled is the C-NOT gate. The C-NOT flips the state of a target (*T*) qubit conditional on a control (C) qubit being in the $|0\rangle$ logical state.

The C-NOT is a notable example of quantum gates since, with one qubit rotations, it is universal for quantum information and, in the photonic implementation, it relies on both quantum and classical interference. For this reason, the performance of the C-NOT gate is a benchmark to evaluate the capabilities of the technology under study. We tested the implementation shown in Fig. 10 [46], [47]. This scheme has previously been experimentally demonstrated using bulk optics [19], [48]–[51], using different ingenious methods to avoid instability in the classical interference. The waveguide implementation, however, is essentially a simple direct-write onto the chip from the theoretical schematic.

The gate works as follow: control C and target T qubits are each encoded by a photon in two waveguides. Two $1/2$ splitters in target waveguides (T_0 and T_1) forms a balanced

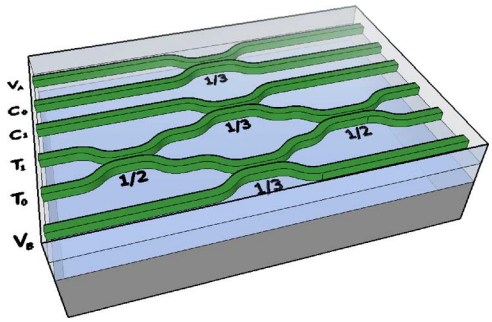

Fig. 10. Schematic representation of an integrated C-NOT gate.

Mach–Zehnder interferometer, so that, with no inputs in the control waveguides (or a photon in the control state zero C_0), the target photons exit the interferometer from the same port as the input port.[4] For the control in the state one (photon in the waveguide C_1), the control and target photons interfere nonclassically at the central $1/3$ splitter. For such a value of splitting ratio, the resulted state evolves to $|1\rangle_C\,|0\rangle_T \rightarrow -1/3(|1\rangle_C\,|0\rangle_T)$. This causes a π-phase difference between the arms of the interferometer, so that the target qubit is flipped. The presented scheme does not always work, it is possible, for example, to find two photons in the control or target outputs. However, the presence of only one photon in the control and one photon in the target herald the success of the gate. The probability of such an event is equal to 1/9 for all the possible combinations of inputs states.

To test the performance of the C-NOT gate, we input the four computational basis states $|0\rangle_C|0\rangle_T$, $|0\rangle_C|1\rangle_T$, $|1\rangle_C|0\rangle_T$, and $|1\rangle_C|1\rangle_T$ and measured the probability of detecting each of the computational basis states at the output [see Fig. 11(a)]. The excellent agreement for the $|0\rangle_C$ inputs (peak values of 98.5%) is a measure of the classical interference in the target interferometer and demonstrates that the waveguides are stable on a subwavelength scale—a key advantage arising from the monolithic nature of an integrated optics architecture. The average of the logical basis fidelities is $F = 94.3 \pm 0.2\%$.

To perform a deeper study of the integrated C-NOT gate, and to prevent possible design and fabrication imperfections, a lithography tuning was made on the reflectivity of the couplers that constitutes the gate. The "1/2" couplers have reflectivity in the range $\eta = 0.4 - 0.6$ in steps of 0.05. The reflectivity of the "1/3" couplers varies accordingly with the reflectivity of the "1/2" ones, in such a way that if the "1/2" has $\eta_{1/2} = 0.5$ then $\eta_{1/3} = 0.33$. For this reason, the values of $\eta_{1/3}$ are $\{0.453, 0.392, 0.333, 0.277, 0.224\}$. Nonclassical two-photon interference experiments were conducted on each of the couplers that constitute the C-NOT gates, the results are reported in Fig. 5(b) (black points representing "1/2" couplers and red points "1/3" couplers). Each C-NOT gate was then tested, reconstructing the truthtables in the computational basis. Fig. 12 shows the fidelities for all five devices as a function of the reflectivity of the "1/2" couplers of the gates. The best fit follows well

[4]Note that for the rest of this paper, we use the convention $U_{\rm dc} = H$, this involves just the relabeling of the output waveguides.

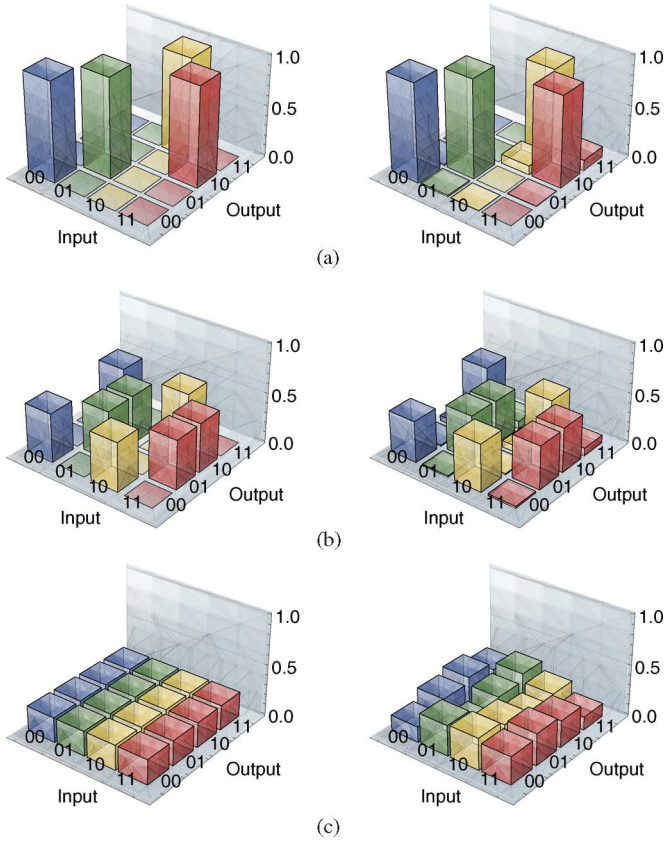

Fig. 11. Characterization of integrated quantum photonic circuits. (a) Ideal (left) and measured (right) truth tables for a C-NOT circuit. (b) C-NOT with two additional H gates. (c) C-NOT with one additional H gate.

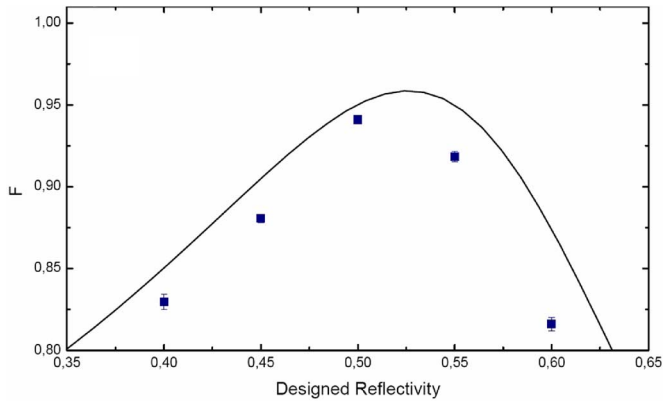

Fig. 12. Fidelity of the C-NOT gate as a function of the reflectivity of the couplers that constitute the device.

the trend of the experimental points, the discrepancy between them is attributed to the fact that the theoretical model used for the best fit does not take into account the nonperfect behavior of the target interferometer.

Performing quantum measurements on the single components of the C-NOT gate, and measuring high fidelity for the operation of the gate with inputs in the computational basis ensures the correct behavior of the integrated chip. However, if we take the quantum discrimination theory point of view and look at the chip as a black box (not using any information we have about

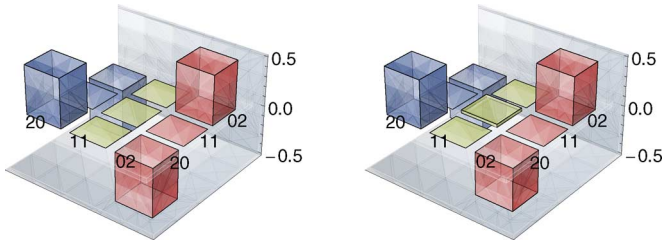

Fig. 13. On-chip estimation of the density matrix for the entangled state $|20\rangle - |02\rangle$, ideal (left) and estimated (right).

the actual components of the device), it is simple to understand that the fidelity value is not enough to fully characterize the quantum gate. To perform such a characterization, quantum process tomography is needed. Unfortunately, at the present stage process tomography for a two qubit operation is hard to implement in path encoding, directly on the chip, since it requires many Mach–Zehnder interferometers and phase shifters to be controlled at the same time. An experimental method was conceived to confirm on-chip coherent quantum operation and entanglement, the most important properties of the C-NOT gate.

Two single photons were launched into the T_0 and T_1 waveguides. The state after the first 1/2 coupler should evolve to

$$|11\rangle_{T_0T_1} \rightarrow (|20\rangle_{T_0T_1} - |02\rangle_{T_0T_1})/\sqrt{2} \tag{9}$$

that is, the entangled state also used in the previous section for quantum metrology. Using part of the circuit that composes the C-NOT gate, it is possible to estimate the fidelity between the desired state and the state produced into the chip. Various combinations of coincidental detections of two photons at the outputs are used for the estimation. The heuristic explanation of the argument is the following: measuring the photon rates at C_1 and V_A allow us to evaluate the diagonal elements of the density matrix. A low rate of coincidental detections of two photons between C_1 and V_A outputs translate to a low $|11\rangle$ component in the state, meanwhile a high rate of two-photon detections in either of these output waveguides (measured using a pair of cascaded detectors) ensures that the state is predominantly composed of $|20\rangle$ and $|02\rangle$ components. These measurements, however, do not give any information about the coherence of the state. At the second 1/2 coupler between the T_0 and T_1 waveguides the reverse transformation of (9) should occur, provided the minus sign of the superposition exists. A high rate of detecting one photon in each of the T_0 and T_1 outputs combined with a low rate of two-photon detections in either of these outputs confirms this transformation. The aforementioned measured count rates, and a worst case scenario for the state evolution, were used to estimate the density matrix of the state after the first 1/2 coupler directly on-chip, the results are shown in Fig. 13. It was not possible to estimate all the coherence elements of the matrix, however, the amount of the unmeasured elements is limited by the small $|11\rangle\langle 11|$ population. Also, it was not possible to distinguish between nonmaximal coherences and rotated coherences with imaginary parts for the $|20\rangle\langle 02|$ and $|02\rangle\langle 20|$ terms. However, neither of these effects changes the state fidelity. The final density matrix show a fidelity with the expected entangled state $|20\rangle - |02\rangle$ of $> 92\%$. This high fidelity generation of the lowest order maximally path entangled state confirms coherent quantum operation and entanglement generation in the chip.

Other simple quantum photonic circuits were tested to show the flexibility of the integrated approach. The devices, shown in Fig. 11(b) and (c), consist of a C-NOT gate and Hadarmard H gates each implemented with a 50:50 coupler between the C_0 and C_1 waveguides. We quantify the agreement between the experimental data and the ideal operation by using the average classical fidelity between probability distributions S [52], [53]. For the data shown in Fig. 11(b), that should produce equal superpositions of the four computation basis states $|00\rangle \pm |01\rangle \pm |10\rangle \pm |11\rangle$, the average classical fidelity with the ideal case was measured to be $S = 97.9 \pm 0.4\%$. The device shown in Fig. 11(c) is an interesting device, since it should produce the four maximally entangled Bell states $\Psi^{\pm} \equiv |10\rangle \pm |01\rangle$ and $\Phi^{\pm} \equiv |00\rangle \pm |11\rangle$. For this device, the similarity with the ideal case was measured to be $S = 91.5 \pm 0.2\%$. While the presence of the entangled state at the output cannot be confirmed directly on-chip, the aforementioned demonstrations of excellent logical basis operation of the C-NOT and coherent quantum operation provides great confidence.

VII. Future Directions of Quantum Integrated Technologies

The results presented in this paper are the first demonstrations of quantum information science experiments using an integrated waveguide platform. The devices investigated were fabricated using well established processing techniques, originally developed for the manufacture of components for the telecommunication market. Although the silica-on-silicon material system is an excellent choice for fabrication of these devices, future integrated quantum photonic devices are likely to take advantage of the wide range of material systems currently available for the fabrication of classical photonic devices.

The challenges for the next generation of quantum photonic devices will focus on increasing the component density, adding functionality and integrating both active and passive quantum elements onto a single device. To achieve this goal, a fully integrated quantum photonic circuit is envisaged; a discrete device comprising single photon emitters, single photon detectors, and quantum logic processing circuits, all integrated onto a single chip.

High component density and compact circuits are crucial for the realization of quantum circuits with complex functionalities. Material systems such as InP, GaAs, or silicon allow the fabrication of waveguides with much higher refractive index contrasts than typically possible with silica waveguides. It is, therefore, possible to fabricate waveguides in these material systems that tightly confine the optical mode and allow for very small bend radius, and thus ultracompact circuits can be realized. Photonic crystal structures are the ultimate approach to reducing the device dimensions, and provide unprecedented control over the propagation of the light on a wavelength scale [54]. These

structures are expected to be key in the future development of quantum photonic circuits.

The photolithographic material processing technologies often used to fabricate photonic devices are restricted to waveguide structures in two dimensions (i.e., planar structures). One approach to increase the complexity of the quantum circuits is to move from this planar layout to a 3-D scheme. Direct write laser waveguide technologies enable the formation of such 3-D structures [55], which can be applied to a wide range of material systems and allows for rapid fabrication of complex 3-D waveguide networks [56]. This technology allows for quantum circuits and architectures that are either impractical or impossible to implement in bulk optics or 2-D waveguide circuits. First characterizations of laser written photonic quantum circuits are under study, showing very promising results [57].

Accurate phase control and reconfigurable circuits are key requirements for future implementation of versatile quantum photonic devices. The device investigated in Section V demonstrated the functionality of a variable beamsplitter, a crucial component in any reconfigurable quantum photonic system. This device was realized in silica using a heater element to control the phase within one arm of the Mach–Zehnder interferometer. As a promising alternative to silica, lithium niobate ($LiNbO_3$) can be used to form low- loss waveguide structures and also exhibits an electrooptic effect, which allows for fast control over the refractive index (tens of gigahertz), as well the possibility to control polarization within waveguide structures. Such fast nonlinearity will be required for the development of integrated photonic devices for feed-forward cluster-state quantum computation (which are currently implemented using bulk optics) [58]. In addition, periodically poled $LiNbO_3$ can be used for highly efficient single photon generation through parametric down conversion, and is an ideal source of single photons for integration with waveguide circuits [59].

The implementations of integrated quantum photonic circuits presented in this paper rely on path encoding schemes. Enhanced flexibility could be achieved by moving toward polarization encoding schemes. Although relatively straight forward to implement in bulk optic schemes, achieving polarization diversity in integrated optics requires complex processing steps and extremely tight control of fabrication tolerances to realize reliable polarization splitters and rotators [60]. It is likely that in the near future the majority of integrated quantum circuits will rely on path encoding, but the possibility of more complex encoding schemes in waveguides, such as polarization, should not be ruled out.

The true potential of the integration approach will only be fully realized when it is possible to integrate active elements, such as sources, detectors, and photonic modules for true light–matter interactions [61]. Integrated single photon sources could be realized through a combination of approaches in waveguides, such as spontaneous parametric down conversion [59], quantum dots [62], and color center sources [63]. Photon number resolving detectors could be implemented through integrated avalanche photodiodes [64] or integrated superconducting detectors [65].

The circuits presented in this paper have demonstrated a modest level of component integration, with the C-NOT gate comprising a total of seven directional couplers. In terms of the possible levels of integration that could be achieved in the near future, we can look towards a selection of recent achievements in integrated telecommunications devices. Using the InP material system, Luxtera have developed a fully integrated silicon based 40 Gb/s transceiver, compatible with the CMOS technology and enabling both optical and electronic functionality to exist on a single chip [66]. Large-scale integration in optically active material systems such as InP and GaAs have been realized by companies such as Infinera, who have achieved component densities in excess of 240 per device [67]. These world-leading technologies demonstrate the levels of integration that are currently possible in classical photonics, and paves the way for the realization of equally large-scale and complex quantum photonic devices. Applying these concepts to quantum optics circuits will not only provide similar advantages in terms of size and scalability, but will also allow for precision, control and complexities previously not possible in quantum optic circuits.

VIII. Conclusion

This paper has presented a new approach in the way optical quantum information science experiments are conducted. Quantum optics experiments have typically been performed with large-scale (bulk) optical elements, and although these systems provide proof-of-principle experiments, they are limited in terms of scalability, stability and complexity and will ultimately hinder the development of more advanced quantum circuits. For quantum optic technologies to flourish, an integration approach must be taken, enabling the development of compact and efficient quantum optic components with unprecedented complexity.

We have presented a selection of proof-of-concept experiments, highlighting the potential of the integration technology for key quantum technologies. On-chip quantum interference has been demonstrated with a maximum visibility of 0.982 ± 0.009. Quantum metrology experiments has been demonstrated using a MZI and two and four photons entangled states, showing fringe contrast of $C = 98.2 \pm 0.3\%$ and $C = 92 \pm 4\%$, respectively. A quantum logic C-NOT gate has also been realized, showing a fidelity in the computational basis of $F = 94.3 \pm 0.2\%$. These components form the building blocks required to realize more complex quantum integrated circuits.

This on-chip control of light at the quantum level will enable new scientific developments in the field of quantum optics, as well as the development of advanced quantum systems for the purposes of quantum metrology, quantum communications and quantum computation.

Acknowledgment

The authors would like to thank A. Laing, M. J. Cryan, J. G. Rarity, and S. Yu for helpful discussions.

REFERENCES

[1] A. Politi, M. J. Cryan, J. G. Rarity, S. Yu, and J. L. O'Brien, "Silica-on-silicon waveguide quantum circuits," *Science*, vol. 320, pp. 646–649, 2008.

[2] J. C. F. Matthews, A. Politi, A. Stefanov, and J. L. O'Brien, "Manipulation of multiphoton entanglement in waveguide quantum circuits," *Nat. Photon.*, vol. 3, pp. 346–350, 2009.

[3] J. J. Sakurai, *Modern Quantum Mechanics*, 2nd ed. Reading, MA: Addison-Wesley, 1994.

[4] M. A. Nielsen and I. L. Chuang, *Quantum Computation and Quantum Information*. Cambridge, U.K.: Cambridge Univ. Press, 2000.

[5] P. Shor, "Algorithms for quantum computation: discrete logarithms andfactoring," in *Proc. 35th Annu. Symp. Found. Comput. Sci.*, Nov., 1994, pp. 124–134.

[6] D. P. DiVincenzo and D. Loss, "Quantum information is physical," *Superlatt. Microstruc.*, vol. 23, pp. 419–432, 1998.

[7] U.S. Advanced Research and Development Activity (ARDA). *Quantum Computation Roadmap for current state- of-the-art*. (2004). [Online]. Available: http://qist.lanl.gov/qcomp_map.shtml

[8] J. L. O'Brien, "Optical quantum computing," *Science*, vol. 318, no. 5856, pp. 1567–1570, 2007.

[9] E. Knill, R. Laflamme, and G. J. Milburn, "A scheme for efficient quantum computation with linear optics," *Nature*, vol. 409, pp. 46–52, 2001.

[10] N. Gisin, G. Ribordy, W. Tittel, and H. Zbinden, "Quantum cryptography," *Rev. Mod. Phys.*, vol. 74, pp. 145–195, 2002.

[11] See the recent demonstration of the SECOQC network in Vienna. (2008). [Online]. Available: www.secoqc.net

[12] V. Giovannetti, S. Lloyd, and L. Maccone, "Quantum-enhanced measurements: Beating the standard quantum limit," *Science*, vol. 306, pp. 1330–1336, 2004.

[13] M. W. Mitchell, J. S. Lundeen, and A. M. Steinberg, "Super-resolving phase measurements with a multiphoton entangled state," *Nature*, vol. 429, no. 6988, pp. 161–164, 2004.

[14] P. Walther, J.-W. Pan, M. Aspelmeyer, R. Ursin, S. Gasparoni, and A. Zeilinger, "De Broglie wavelength of a non-local four-photon state," *Nature*, vol. 429, no. 6988, pp. 158–161, 2004.

[15] T. Nagata, R. Okamoto, J. L. O'Brien, K. Sasaki, and S. Takeuchi, "Beating the standard quantum limit with four-entangled photons," *Science*, vol. 316, no. 5825, pp. 726–729, 2007.

[16] B. L. Higgins, D. W. Berry, S. D. Bartlett, H. M. Wiseman, and G. J. Pryde, "Entanglement-free Heisenberg-limited phase estimation," *Nature*, vol. 450, pp. 393–397, 2007.

[17] A. N. Boto, P. Kok, D. S. Abrams, S. L. Braunstein, C. P. Williams, and J. P. Dowling, "Quantum interferometric optical lithography: Exploiting entanglement to beat the diffraction limit," *Phys. Rev. Lett.*, vol. 85, no. 13, pp. 2733–2736, Sep. 2000.

[18] Y. Kawabe, H. Fujiwara, R. Okamoto, K. Sasaki, and S. Takeuchi, "Quantum interference fringes beating the diffraction limit," *Opt. Exp.*, vol. 15, pp. 14244–14250, 2007.

[19] J. L. O'Brien, G. J. Pryde, A. G. White, T. C. Ralph, and D. Branning, "Demonstration of an all-optical quantum controlled-NOT gate," *Nature*, vol. 426, no. 6964, pp. 264–267, 2003.

[20] A. Einstein, B. Podolsky, and N. Rosen, "Can quantum-mechanical description of physical reality be considered complete?," *Phys. Rev.*, vol. 47, pp. 777–780, 1935.

[21] J. Bell, "On the Einstein Podolsky Rosen paradox," *Physics*, vol. 1, pp. 195–200, 1964.

[22] A. Aspect, P. Grangier, and G. Roger, "Experimental realization of Einstein-Podolsky-Rosen-Bohm gedankenexperiment: A new violation of Bell's inequalities," *Phys. Rev. Lett.*, vol. 49, no. 2, pp. 91–94, Jul. 1982.

[23] A. Aspect, J. Dalibard, and G. Gérard, "Experimental test of Bell's inequalities using time- varying analyzers," *Phys. Rev. Lett*, vol. 49, pp. 1804–1807, 1982.

[24] G. Whihs, T. Jennewein, C. Simon, H. Weinfurter, and A. Zeilinger, "Violations of Bell's inequality under strict Einstein locality conditions," *Phys. Rev. Lett.*, vol. 81, pp. 5039–5043, 1998.

[25] M. A. Rowe, D. Kielpinski, V. Meyer, C. A. Sackett, W. M. Itano, C. Monroe, and D. J. Wineland, "Experimental violation of a Bell's inequality with efficient detection," *Nature*, vol. 409, pp. 791–794, 2001.

[26] D. Bouwmeester, J.-W. Pan, K. Mattle, M. Eibl, H. Weinfurter, and A. Zeilinger, "Experimental quantum teleportation," *Nature*, vol. 390, pp. 575–579, 1997.

[27] D. Boschi, S. Branca, F. De Martini, L. Hardy, and S. Popescu, "Experimental realization of teleporting an unknown pure quantum state via dual classical and Einstein-Podolsky-Rosen channels," *Phys. Rev. Lett.*, vol. 80, no. 6, pp. 1121–1125, Feb. 1998.

[28] K. Mattle, H. Weinfurter, P. G. Kwiat, and A. Zeilinger, "Dense coding in experimental quantum communication," *Phys. Rev. Lett.*, vol. 76, pp. 4656–4659, 1996.

[29] P. Walther, K. J. Resch, T. Rudolph, E. Schenck, H. Weinfurter, V. Vedral, M. Aspelmeyer, and A. Zeilinger, "Experimental one-way quantum computing," *Nature*, vol. 434, no. 7030, pp. 169–176, 2005.

[30] C.-Y. Lu, X.-Q. Zhou, O. Gühne, W.-B. Gao, J. Zhang, Z.-S. Yuan, A. Gobel, T. Yang, and W.-J. Pan, "Experimental entanglement of six photons in graph states," *Nat. Phys.*, vol. 3, pp. 91–95, 2007.

[31] K. Kato, M. Ishii, and Y. Inoue, "Packaging of large-scale planar lightwave circuits," *IEEE Trans. Compon. Packag. Manuf. Technol. B: Adv. Packag.*, vol. 21, no. 2, pp. 121–129, May 1998.

[32] M. Kawachi, "Silica waveguides on silicon and their application to integrated-optic components," *Opt. Quantum Electron.*, vol. 22, no. 5, pp. 391–416, Sep. 1990.

[33] T. Honjo, K. Inoue, and H. Takahashi, "Differential-phase-shift quantum key distribution experiment with aplanar light-wave circuit mach-zehnder interferometer," *Opt. Lett.*, vol. 29, no. 23, pp. 2797–2799, 2004.

[34] H. Takesue and K. Inoue, "Generation of 1.5-μm band time-bin entanglement using spontaneous fiber four-wave mixing and planar light-wave circuit interferometers," *Phys. Rev. A*, vol. 72, no. 4, pp. 041804-1–041804-4, Oct. 2005.

[35] C. K. Hong, Z. Y. Ou, and L. Mandel, "Measurement of subpicosecond time intervals between two photons by interference," *Phys. Rev. Lett.*, vol. 59, pp. 2044–2046, 1987.

[36] P. P. Rohde, G. J. Pryde, J. L. O'Brien, and T. C. Ralph, "Quantum-gate characterization in an extended Hilbert space," *Phys. Rev. A*, vol. 72, no. 3, pp. 032306-1–032306-5, 2005.

[37] M. A. Nielsen and I. L. Chuang *Quantum Computation and Quantum Information*. Cambridge, U.K., Cambridge Univ. Press, 2000, p. 506, ch. 11.

[38] M. Reck, A. Zeilinger, H. J. Bernstein, and P. Bertani, "Experimental realization of any discrete unitary operator," *Phys. Rev. Lett.*, vol. 73, no. 1, pp. 58–61, Jul. 1994.

[39] I. Kenichi and Y. Kokubun, *Encyclopedic Handbook of Integrated Optics*. Boca Raton, FL: CRC Press, 2006.

[40] K. J. Resch, K. L. Pregnell, R. Prevedel, A. Gilchrist, G. J. Pryde, J. L. O'Brien, and A. G. White, "Time-reversal and super-resolving phase measurements," *Phys. Rev. Lett.*, vol. 98, no. 22, pp. 223601-1–223601-4, 2007.

[41] R. Okamoto, H. F. Hofmann, T. Nagata, J. L. O'Brien, K. Sasaki, and S. Takeuchi, "Beating the standard quantum limit: Phase super-sensitivity of n-photon interferometers," *New J. Phys.*, vol. 10, no. 7, pp. 073033-1–073033-9, 2008.

[42] H. Lee, P. Kok, and J. Dowling, "A quantum Rosetta stone for interferometry," *J. Mod. Opt.*, vol. 49, no. 14–15, pp. 2325–2338, 2002.

[43] O. Steuernagel, "de broglie wavelength reduction for a multiphoton wave packet," *Phys. Rev. A*, vol. 65, no. 3, pp. 033820-1–033820-4, Feb. 2002.

[44] K. Sanaka, K. J. Resch, and A. Zeilinger, "Filtering out photonic Fock states," *Phys. Rev. Lett.*, vol. 96, no. 8, pp. 083601-1–083601-4, 2006.

[45] K. J. Resch, J. L. O'Brien, T. J. Weinhold, K. Sanaka, B. P. Lanyon, N. K. Langford, and A. G. White, "Entanglement generation by Fock-state filtration," *Phys. Rev. Lett.*, vol. 98, no. 20, pp. 203602-1–203602-4, 2007.

[46] T. C. Ralph, N. K. Langford, T. B. Bell, and A. G. White, "Linear optical controlled-NOT gate in the coincidence basis," *Phys. Rev. A*, vol. 65, pp. 062324-1–062324-5, 2001.

[47] H. F. Hofmann and S. Takeuchi, "Quantum phase gate for photonic qubits using only beam splitters and postselection," *Phys. Rev. A*, vol. 66, pp. 024308-1–024308-3, 2001.

[48] J. L. O'Brien, G. J. Pryde, A. Gilchrist, D. F. V. James, N. K. Langford, T. C. Ralph, and A. G. White, "Quantum process tomography of a controlled-NOT gate," *Phys. Rev. Lett.*, vol. 93, no. 8, pp. 080502-1–080502-4, 2004.

[49] N. K. Langford, T. J. Weinhold, R. Prevedel, K. J. Resch, A. Gilchrist, J. L. O'Brien, G. J. Pryde, and A. G. White, "Demonstration of a simple entangling optical gate and its use in Bell-state analysis," *Phys. Rev. Lett.*, vol. 95, no. 21, pp. 210504-1–210504-4, 2005.

[50] N. Kiesel, C. Schmid, U. Weber, R. Ursin, and H. Weinfurter, "Linear optics controlled-phase gate made simple," *Phys. Rev. Lett.*, vol. 95, no. 21, p. 210505, 2005.

[51] R. Okamoto, H. F. Hofmann, S. Takeuchi, and K. Sasaki, "Demonstration of an optical quantum controlled-not gate without path interference," *Phys. Rev. Lett.*, vol. 95, no. 21, pp. 210506-1–210506-4, 2005.
[52] G. J. Pryde, J. L. O'Brien, A. G. White, S. D. Bartlett, and T. C. Ralph, "Measuring a photonic qubit without destroying it," *Phys. Rev. Lett.*, vol. 92, pp. 190402-1–190402-4, 2004.
[53] T. C. Ralph, S. D. Bartlett, J. L. O'Brien, G. J. Pryde, and H. M. Wiseman, "Quantum nondemolition measurements for quantum information," *Phys. Rev. A*, vol. 73, no. 1, pp. 012113-1–012113-11, 2006.
[54] T. F. Krauss and R. M. De La Ru, "Photonic crystals in the optical regime—past, present, and future," *Progr. Quantum Electron.*, vol. 23, no. 2, pp. 51–96, 1999.
[55] K. M. Davis, K. Miura, N. Sugimoto, and K. Hirao, "Writing waveguides in glass with a femtosecond laser," *Opt. Lett.*, vol. 21, no. 21, pp. 1729–1731, 1996.
[56] R. R. Thomson, H. T. Bookey, N. D. Psaila, A. Fender, S. Campbell, W. N. MacPherson, J. S. Barton, D. T. Reid, and A. K. Kar, "Ultrafast-laser inscription of a 3-D fan-out device for multicore fiber coupling applications," *Opt. Exp.*, vol. 15, no. 18, pp. 11 691–11 697, 2007.
[57] G. D. Marshall, A. Politi, J. C. F. Matthews, P. Dekker, M. Ams, M. J. Withford, and J. L. O'Brien, "Laser written waveguide photonic quantum circuits," *Opt. Exp.*, vol. 17, pp. 12546–12554, 2009.
[58] R. Prevedel, P. Walther, F. Tiefenbacher, P. Bohi, R. Kaltenbaek, T. Jennewein, and A. Zeilinger, "High-speed linear optics quantum computing using active feed-forward," *Nature*, vol. 445, no. 7123, pp. 65–69, 2007.
[59] S. Tanzilli, W. Tittel, H. De Riedmatten, H. Zbinden, P. Baldi, M. De Micheli, D. Ostrowsky, and N. Gisin, "PPLN waveguide for quantum communication," *Eur. Phys. J. D*, vol. 18, no. 2, pp. 155–160, Feb. 2002.
[60] L. Augustin, R. Hanfoug, J. van der Tol, W. de Laat, and M. Smit, "A compact integrated polarization splitter/converter in InGaAsP InP," *IEEE Photon. Technol. Lett.*, vol. 19, no. 17, pp. 1286–1288, Sep. 2007.
[61] S. J. Devitt, A. D. Greentree, R. Ionicioiu, J. L. O'Brien, W. J. Munro, and L. C. L. Hollenberg, "Photonic module: An on-demand resource for photonic entanglement," *Phys. Rev. A (At., Mol., Opt. Phys.)*, vol. 76, no. 5, p. 052312, 2007.
[62] T. Lund-Hansen, S. Stobbe, B. Julsgaard, H. Thyrrestrup, T. Sünner, M. Kamp, A. Forchel, and P. Lodahl, "Experimental realization of highly efficient broadband coupling of single quantum dots to a photonic crystal waveguide," *Phys. Rev. Lett.*, vol. 101, no. 11, pp. 113903-1–113903-4, 2008.
[63] A. D. Greentree, B. A. Fairchild, F. M. Hossain, and A. Prawer, "Diamond integrated quantum photonics," *Mater. Today*, vol. 11, no. 9, pp. 22–31, 2008.
[64] K. Tsujino, M. Akiba, and M. Sasaki, "Ultralow-noise readout circuit with an avalanche photodiode: toward a photon-number-resolving detector," *Appl. Opt.*, vol. 46, no. 7, pp. 1009–1014, 2007.
[65] A. Divochiy, F. Marsili, D. Bitauld, A. Gaggero, R. Leoni, F. Mattioli, A. Korneev, V. Seleznev, N. Kaurova, O. Minaeva, G. Gol'tsman, K. G. Lagoudakis, M. Benkhaoul, F. Levy, and A. Fiore, "Superconducting nanowire photon-number-resolving detector at telecommunication wavelengths," *Nat. Photon.*, vol. 2, no. 5, pp. 302–306, May 2008.
[66] A. Narasimha, B. Analui, Y. Liang, T. Sleboda, S. Abdalla, E. Balmater, S. Gloeckner, D. Guckenberger, M. Harrison, R. Koumans, D. Kucharski, A. Mekis, S. Mirsaidi, D. Song, and T. Pinguet, "A fully integrated 4 $\times$ 10-Gb/s DWDM optoelectronic transceiver implemented in a standard 0.13 μm CMOS SOI technology," *IEEE J. Solid-State Circuits*, vol. 42, no. 12, pp. 2736–2744, Dec. 2007.
[67] D. Welch, F. Kish, S. Melle, R. Nagarajan, M. Kato, C. Joyner, J. Pleumeekers, R. Schneider, J. Back, A. Dentai, V. Dominic, P. Evans, M. Kauffman, D. Lambert, S. Hurtt, A. Mathur, M. Mitchell, M. Missey, S. Murthy, A. Nilsson, R. Salvatore, M. Van Leeuwen, J. Webjorn, M. Ziari, S. Grubb, D. Perkins, M. Reffle, and D. Mehuys, "Large-scale InP photonic integrated circuits: Enabling efficient scaling of optical transport networks," *IEEE J. Sel. Topics Quantum Electron.*, vol. 13, no. 1, pp. 22–31, Jan./Feb. 2007.

Alberto Politi received the B.Eng. degree in electrical engineering and M.Phys. degree from the University of Pavia, Pavia, Italy, in 2003 and 2005, respectively. He is currently working toward the Ph.D. degree at the Centre for Quantum Photonics, H. H. Wills Physics Laboratory and Department of Electrical and Electronic Engineering, University of Bristol, Bristol, U.K.

His current research interests include nanostructured devices for light manipulation and photonic integrated circuits for quantum science applications.

Jonathan C. F. Matthews received the M.Sci. degree in mathematics from the School of Mathematics, University of Bristol, Bristol, U.K., in 2005, and the M.Sc. degree in communication systems and signal processing from the Department of Electrical and Electronic Engineering, University of Bristol, in 2008. He is currently working toward the Ph.D. degree at the Centre for Quantum Photonics, H. H. Wills Physics Laboratory, and Department of Electrical and Electronic Engineering, University of Bristol.

His current research interests include integrated waveguide circuits for linear optical quantum technologies.

Mark G. Thompson received the M.Phys. degree in physics from the University of Sheffield, Sheffield, U.K., in 2000, and the Ph.D. degree from the University of Cambridge, Cambridge, U.K., in 2006, for his work on ultra-fast semiconductor optoelectronic devices.

He is currently a Lecturer in the Department of Physics and of Electrical and Electronic Engineering at the University of Bristol, Bristol, U.K, and also a Toshiba Research Fellow with Toshiba Research and Development Centre, Kawasaki, Japan. As a Research Scientist with Bookham Technology Ltd., Oxfordshire, U.K., he was engaged on the development of silicon integrated photonic devices during 2000–2002. He then joined the University of Cambridge, first as a Ph.D. Student and then as a Research Fellow from 2006 to 2008, where he was engaged on the research in quantum-dot optoelectronic devices. His research interests include photonic devices, particularly ultra-fast photonic devices, short pulse generation, silicon integrated photonics, and integrated quantum photonic circuits.

Jeremy L. O'Brien received the Ph.D. degree in physics from the University of New South Wales, Sydney, N.S.W., in 2002 for experimental work on correlated and confined electrons in organic conductors, superconductors, and semiconductor nanostructures, as well as progress toward the fabrication of phosphorus in a silicon quantum computer.

He is currently a Professor of physics and electrical engineering in the Department of Electrical and Electronic Engineering, and the H. H. Wills Physics Laboratory, University of Bristol, Bristol, U.K. As a Research Fellow at the University of Queensland, Brisbane, Qld., Australia, he was engaged on quantum optics and quantum information science with single photons during 2001–2006. At CQP, he has been engaged on the fundamental and applied quantum mechanics at the heart of quantum information science and technology, ranging from prototypes for scalable quantum computing to generalized quantum measurements, quantum control, and quantum metrology.